The lncRNA *APOLO* interacts with the transcription factor WRKY42 to trigger root hair cell expansion in response to cold

Michaël Moison[*1], Javier Martínez Pacheco[*2], Leandro Lucero[*1], Camille Fonouni-Farde[1], Johan Rodríguez-Melo[3], Aurélie Christ[4], Jérémie Bazin[4]; Moussa Benhamed[4]; Fernando Ibañez[3], Martin Crespi[4], José M. Estevez[†,2,5] and Federico Ariel[†1]

[1] Instituto de Agrobiotecnología del Litoral, Universidad Nacional del Litoral, CONICET, FBCB/FHUC, Centro Científico Tecnológico CONICET Santa Fe, Colectora Ruta Nacional No 168 km. 0, Paraje El Pozo, Santa Fe 3000, Argentina.

[2] Fundación Instituto Leloir and IIBBA-CONICET, Av. Patricias Argentinas 435, Buenos Aires CP C1405BWE, Argentina.

[3] Instituto de Investigaciones Agrobiotecnológicas, CONICET, Universidad Nacional de Río Cuarto, Río Cuarto 5800, Argentina.

[4] Institute of Plant Sciences Paris-Saclay (IPS2), CNRS, INRA, University Paris-Saclay and University of Paris Bâtiment 630, 91192 Gif sur Yvette, France.

[5] Centro de Biotecnología Vegetal (CBV), Facultad de Ciencias de la Vida (FCsV), Universidad Andres Bello, Santiago, Chile and Millennium Institute for Integrative Biology (iBio), Santiago, Chile.

[*] These authors contributed equally to this work

[†] Correspondence to: Federico Ariel (fariel@santafe-conicet.gov.ar) and José M. Estevez (jestevez@leloir.org.ar)

Text Word count (without Abstract and References)**:** 5,699

ABSTRACT

Plant long noncoding RNAs (lncRNAs) have emerged as important regulators of chromatin dynamics, impacting on transcriptional programs leading to different developmental outputs. The lncRNA *AUXIN REGULATED PROMOTER LOOP* (*APOLO*) directly recognizes multiple independent loci across the *Arabidopsis* genome and modulates their three-dimensional chromatin conformation, leading to transcriptional shifts. Here, we show that *APOLO* recognizes the locus encoding the root hair (RH) master regulator ROOT HAIR DEFECTIVE 6 (RHD6) and controls *RHD6* transcriptional activity leading to cold-enhanced RH elongation. Furthermore, we demonstrate that *APOLO* interacts with the transcription factor WRKY42 and modulates its binding to the *RHD6* promoter. WRKY42 is required for the activation of *RHD6* by low temperatures and *WRKY42* deregulation impairs cold-induced RH expansion. Collectively, our results indicate that a novel ribonucleoprotein complex involving *APOLO* and WRKY42 forms a regulatory hub which activates *RHD6* by shaping its epigenetic environment and integrates signals governing RH growth and development.

Words: 148

Key words: root hairs; cell expansion; long noncoding RNAs; *APOLO*; transcription factors; RHD6; WRKY42; cold temperature

45 **INTRODUCTION**

46

47 Root hairs (RHs) are single cell projections developed from specialized epidermal trichoblast cells
48 able to increase their size several hundred times in a polar manner to reach and promote the uptake of
49 water-soluble nutrients, interact with soil microorganisms and support anchor to the plant. The specifica-
50 tion of epidermal cells into RHs is a complex process whose underlying mechanisms are partially under-
51 stood. In *Arabidopsis thaliana*, RH cell fate is controlled by a developmental program involving a complex
52 of transcription factors (TFs) promoting the expression of the homeodomain protein GLABRA 2 (GL2) (Ryu
53 et al., 2005; Song et al., 2011; Schiefelbein et al., 2014; Balcerowicz et al., 2015). GL2 blocks RH develop-
54 ment by inhibiting the transcription of the master regulator *ROOT HAIR DEFECTIVE 6* (*RHD6*) (Lin et al.,
55 2015). In the cells that differentiate into RHs (known as trichoblasts), a second TF complex suppresses *GL2*
56 expression (Schiefelbein et al., 2014), forcing the cells to enter the RH cell fate program via the concomi-
57 tant activation of RHD6 along with downstream TFs (Menand et al., 2007; Pires et al., 2013). Briefly, RHD6
58 together with its homolog RSL1 (ROOT HAIR DEFECTIVE 6 LIKE 1) induce the expression of TFs from the
59 bHLH family, including RSL2 (ROOT HAIR DEFECTIVE 6 LIKE 2) and RSL4 (ROOT HAIR DEFECTIVE 6 LIKE 4),
60 ultimately triggering the differentiation of the RHs and their subsequent polarized tip-growth (Karas et al.,
61 2009; Yi et al., 2010; Bruex et al., 2012). In addition, it was proposed that RSL4 controls the expression of
62 a small subset of nearly 125 genes (Won et al., 2009; Yi et al., 2010; Datta et al., 2015; Vijayakumar et al.,
63 2016), including several cell wall extensins (EXTs) (Ringli, 2010; Velasquez et al., 2011) sufficient to pro-
64 mote RH growth (Hwang et al., 2017).

65 RH expansion is regulated both by cell-intrinsic factors (e.g. endogenous phytohormones such as
66 auxin) and external environmental signals (e.g. phosphate (Pi) availability in the soil) (Mangano et al., 2017;
67 Bhosale et al., 2018). Pi starvation is one of the key environmental factors promoting rapid RH growth (Yi
68 et al., 2010; Datta et al., 2015; Vijayakumar et al., 2016). In *Arabidopsis*, it triggers *RSL4* expression via an
69 enhanced auxin production, activating downstream effector genes mediating cell growth (Yi et al., 2010;
70 Datta et al., 2015; Mangano et al., 2017; Marzol et al., 2017; Bhosale et al., 2018). Accordingly, several
71 auxin-related TFs have been implicated in Pi-starvation signaling in roots, including WRKY proteins that
72 control the expression of the Pi transporter families Pi-permease PHO1 and PHOSPHATE TRANSPORTER
73 (PHT) (Devaiah et al., 2007; Chen et al., 2009; Wang et al., 2014; Su et al., 2015). Under Pi-sufficient con-
74 ditions, WRKY6 and WRKY42 bind to W-boxes of the *PHO1* promoter and suppress its expression. During
75 Pi starvation, WRKY42 is degraded by the 26S proteasome pathway, resulting in the activation of *PHO1*
76 transcription (Chen et al., 2009; Su et al., 2015). In addition, WRKY42 functions as a positive regulator of

77 *PHT1;1*, by binding to its promoter under Pi-sufficient condition (Su et al., 2015). Overall, WRKY42 is part
78 of the components activating root early-responses to Pi starvation, although its role in controlling RH
79 growth remains unexplored.

80 In recent years, plant long noncoding RNAs (lncRNAs) have emerged as important regulators of
81 gene expression, and several among them, have been functionally linked to Pi homeostasis. For instance,
82 the lncRNA *INDUCED BY PHOSPHATE STARVATION 1* (*IPS1*) can sequester the Pi starvation-induced mi-
83 croRNA miR-399, attenuating miR-399-mediated repression of *PHO2*, a gene involved in Pi uptake (Franco-
84 Zorrilla et al., 2007). In addition, the *cis*-natural antisense (*cis*-NAT) transcript *PHO1;2*, induced under Pi
85 deficiency, was shown to promote the translation of the *PHO1;2* mRNA involved in Pi loading into the
86 xylem. The expression of this *cis*-NAT is associated with the transport of the sense–antisense RNA pair
87 toward the polysomes (Jabnoune et al., 2013). More recently, it was shown that the lncRNA *AUXIN REGU-*
88 *LATED PROMOTER LOOP* (*APOLO*) recognizes multiple spatially independent genes by sequence comple-
89 mentarity and DNA-RNA duplex formation, known as R-loops. Upon recognition, *APOLO* shapes the three-
90 dimensional (3D) conformation of its target regions by decoying the Polycomb Repressive Complex 1
91 (PRC1) component LIKE HETEROCHROMATIN PROTEIN 1 (LHP1), thereby regulating their transcription
92 (Ariel et al., 2014; Ariel et al., 2020).

93 Here, we show that the lncRNA *APOLO* directly regulates a subset of genes involved in RH devel-
94 opment, including the master regulator of RH initiation *RHD6*. *APOLO* activates *RHD6* transcription by
95 modulating the formation of a local chromatin loop encompassing its promoter region, an epigenetic reg-
96 ulatory mechanism likely involving PRC1 and PRC2 components. Furthermore, we found that *APOLO* inter-
97 acts with the TF WRKY42, forming a new hub that regulates *RHD6* to induce RH growth in response to low
98 temperatures.

99

100 **RESULTS**

101

102 ***APOLO* regulates root hair cell elongation in response to low temperatures**

103 Based on Chromatin Isolation by RNA Purification (ChIRP-Seq) performed in wild-type (WT) plants,
104 it was previously reported that the lncRNA *APOLO* recognizes a subset of independent loci enriched in
105 categories related to cell wall composition and organization (Ariel et al., 2020). A closer look at *APOLO bona*
106 *fide* targets allowed us to identify seventeen genes involved in RH growth and expansion (**Supplementary**
107 **Table 1**), a process dependent on cell wall remodeling molecules, including EXTs and EXT-related proteins

108 (Ringli, 2010; Lamport et al., 2011; Velasquez et al., 2011; Velasquez et al., 2015; Marzol et al., 2018). In-
109 terestingly, according to single-cell RNA-seq datasets (Zhang et al., 2019) *APOLO* transcripts are enriched
110 in RH cells (**Supplementary Figure 1A**). Notably, sixteen *APOLO* direct targets were upregulated upon
111 *APOLO* over-expression (**Supplementary Table 2**). Furthermore, 52 additional RH-related genes were up-
112 regulated in *35S:APOLO* seedlings (**Supplementary Table 2**) (Ariel et al., 2020). Among them, the RH central
113 TFs *RHD6* (as a direct target), *RSL2* and *RSL4* (as indirectly regulated) were induced upon *APOLO* over-ex-
114 pression.

115 It was reported that the *APOLO* locus is targeted by the RNA-polymerase Pol V and silenced by
116 RNA-directed DNA Methylation (RdDM,(Ariel et al., 2014)). A search in a small RNA-Seq performed in WT
117 roots subjected to different temperature treatments (Gyula et al., 2018) revealed that RdDM-related 24nt
118 siRNA accumulation over the *APOLO* locus is less abundant at low temperatures (**Supplementary Figure**
119 **1B**), suggesting that *APOLO* transcription is regulated by cold. Accordingly, we found that *APOLO* transcrip-
120 tional accumulation increases in roots after 24h at 10°C (**Figure 1A**). An analysis of the promoter activity of
121 the 5.2kb region upstream *APOLO* (Ariel et al., 2020) directing the expression of a *GFP* reporter gene, ad-
122 ditionally revealed a higher transcriptional activity at low temperatures in the RHs (**Figure 1B**). Strikingly,
123 we observed that two RNAi-*APOLO* and *35S:APOLO* independent lines (Ariel et al., 2014; Ariel et al., 2020)
124 exhibit a basal increase of RH length at 22°C, and uncovered a strong induction of RH elongation in WT and
125 RNAi-*APOLO* at 10°C, in contrast to *35S:APOLO* lines (**Figure 1C**). Accordingly, *RHD6* is induced in response
126 to cold in WT roots and RNAi-*APOLO* roots display higher *RHD6* basal levels than the WT (**Figure 1D**). Col-
127 lectively, our findings suggest that *APOLO* participates in the induction of cold-mediated RH elongation and
128 a deregulation of *APOLO* transcript levels can impact RH growth.

129 Previous studies pointed out a key role of RHD6 (together with RSL1) in RH development, which is
130 mediated by RSL4 and RSL2 as downstream regulators of RH cell elongation (Menand et al., 2007; Pires et
131 al., 2013). Notably, *RHD6*, *RSL2* and *RSL4* transcript levels were upregulated in *35S:APOLO* seedlings (**Sup-**
132 **plementary Table 2**; (Ariel et al., 2020)). Thus, we assessed if these TFs were also controlling the promotion
133 of RH growth by low temperatures. To this end, we tested how *rhd6/rsl1/rsl4* and *rsl2*, *rsl4* and double
134 mutant plants *rsl2/rsl4* respond to low temperatures in comparison with control conditions **(Supplemen-**
135 **tary Figure 2A)**. The *rsl2* mutant was highly responsive to low temperatures in a similar manner to WT
136 while *rsl4* was impaired in the response to cold. The double mutant *rsl2/rsl4* and the triple mutant
137 *rhd6/rsl1/rsl4* did not develop RHs in either of the two conditions. In addition, constitutive expression of
138 *RSL4* (*35S:RSL4*) as well as its expression under the control of the RH specific *EXPANSIN7* promoter
139 (*EXP7p:RSL4*) boosted basal RH growth without further enhancement in response to cold (**Supplementary**

140 **Figure 2B**). These results demonstrate that RSL4 is largely required for RHD6-dependent activation of RH
141 growth at low temperature, and RSL2 might participate to a lower extent.
142 Nutrient availability is known to activate RH expansion through a transcriptional reprogramming
143 governed by RHD6 and downstream TFs. The quantification of RH growth of WT plants in response to in-
144 creasing concentrations of nutrients (0.5X to 2.0X MS (Murashige and Skoog) medium) indicates that high
145 concentrations of nutrients completely abolish RH growth triggered by low temperatures **(Supplementary**
146 **Figure 3A**). In a similar way, by increasing agar concentration in the MS medium (from 0.8% to 2.5%) re-
147 straining nutrient mobility, cold-induced RH is clearly blocked **(Supplementary Figure 3B**). Altogether,
148 these observations suggest that low temperatures restrict nutrient mobility and availability in the culture
149 medium, leading to the promotion of polar RH growth.

150

151 ***APOLO* directly modulates the three-dimensional chromatin conformation of the root hair specific locus**
152 ***RHD6***

153 Among *APOLO* targets involved in RH development, we found the master regulator of RH initiation
154 *RHD6* (Menand et al., 2007; Pires et al., 2013). The epigenetic profile of the *RHD6* locus corresponds to
155 typical *APOLO* targets (**Figure 2A**, (Ariel et al., 2020)), including H3K27me3 deposition (track 1), LHP1 recog-
156 nition (track 2, chromatin immunoprecipitation (ChIP)-Seq, (Veluchamy et al., 2016)), and *APOLO* binding
157 regions (tracks 3 to 5, chromatin isolation by RNA purification (ChIRP)-Seq, (Ariel et al., 2020)). A GAAGAA
158 box, shown to be important for *APOLO* target recognition (Ariel et al., 2020) is located in the *RHD6* locus
159 and coincides with *APOLO* binding site. In addition, a peak of DNA-RNA hybrid immunoprecipitation (DRIP)-
160 Seq from root samples indicates the presence of an R-loop coinciding with *APOLO* recognition sites over
161 *RHD6* (tracks 6 to 8, (Xu et al., 2020)).
162 Remarkably, *APOLO* recognition and R-loop formation are also detectable over *RHD6* neighbor
163 gene, located 3.2 kb upstream *RHD6* transcription start site (**Figure 2A**). According to *Dpn*II Hi-C datasets
164 from Arabidopsis seedlings (Liu et al., 2016), a chromatin loop encompassing the intergenic region up-
165 stream *RHD6* was detected (**Figure 2B**), and coincides with *APOLO* binding-sites (**Figure 2A**, ChIRP-Seq). By
166 performing a ChIRP-qPCR with two independent set of biotinylated probes to purify *APOLO* (ODD and
167 EVEN; (Ariel et al., 2020)) and one additional set used as a negative control (LacZ), we confirmed that
168 *APOLO* RNA–*RHD6* DNA interaction occurs in WT and is lost in *APOLO* knockdown (RNAi) seedlings ((Ariel
169 et al., 2014); **Figure 2C**). In addition, the quantification of relative *RHD6* loop formation in RNAi-*APOLO* and
170 *APOLO* over-expressing (*35S:APOLO*; (Ariel et al., 2020)) seedlings, revealed impaired loop formation in

171 both lines (**Figure 2D**), hinting at a stoichiometric requirement of *APOLO* for *RHD6* chromatin loop for-
172 mation. Accordingly, RNA-Seq dataset of *35S:APOLO* seedlings *vs.* WT (Ariel et al., 2020) indicates that
173 *RHD6* transcript levels are increased upon *APOLO* over-expression (**Figure 2E, Supplementary Table 1**),
174 suggesting that the chromatin loop including *RHD6* promoter region precludes transcription. Altogether,
175 our results indicate that *APOLO* lncRNA directly regulates *RHD6* transcriptional activity by fine-tuning local
176 chromatin 3D conformation.

177 It was previously reported that PRC2 actively participates in the regulation of RH growth (Ikeuchi
178 et al., 2015) and that the *RHD6* locus exhibits H3K27me3 deposition and LHP1 recognition (**Figure 2A;**
179 (Veluchamy et al., 2016)). Considering that the lncRNA *APOLO* interacts with the PRC1 component LHP1 *in*
180 *vivo* (Ariel et al., 2014; Ariel et al., 2020), we decided to explore the role of PRC1 and PRC2 in *APOLO*-
181 mediated *RHD6* activation at low temperatures. At 22°C, *RHD6* suffers a reduction of H3K27me3 in the
182 PRC2 mutant *curly leaf* (*clf*), in contrast to the PRC1 mutant *lhp1* (**Supplementary Figure 4A;** (Veluchamy
183 et al., 2016)). Interestingly, we observed that H3K27me3 deposition and LHP1 binding diminish in WT roots
184 treated for 24h at 10°C compared to 22°C (**Supplementary Figure 4B**), consistent with the induction of
185 *RHD6* in response to cold (**Figure 2E**). Moreover, *lhp1* and *clf* mutants exhibit a basal decrease of RH length
186 together with a slight decrease of cold-induced RH elongation in *lhp1*, and a strong decrease of cold-in-
187 duced RH elongation in *clf* (**Supplementary Figure 4D**). Consistently, *RHD6* transcriptional activation by
188 cold is abolished in the *clf* mutant (**Supplementary Figure 4C**), hinting at an important role of chromatin
189 rearrangement for *RHD6* activation in response to cold.
190

191 ***APOLO* interacts with the transcription factor WRKY42 to coordinate the activation of *RHD6***

192 With the aim of uncovering novel actors involved in cold-induced transcriptional regulation of RH
193 growth, we aimed at identifying *APOLO* protein partners. To this end, we performed an exploratory ChIRP
194 on WT seedlings using two independent set of biotinylated probes to purify *APOLO* (ODD and EVEN; (Ariel
195 et al., 2014; Ariel et al., 2020)), and one additional set used as a negative control (against LacZ), as recently
196 described (Rigo et al., 2020). Co-purified proteins were precipitated and analyzed by mass spectrometry.
197 Among the potential *APOLO* partners (i.e. identified with at least two hits in ODD and EVEN samples, but
198 absent in LacZ-ChIRP), we found the WRKY42 protein, a TF involved in the response to Pi starvation (Su et
199 al., 2015), an environmental condition that promotes RH cell expansion (Bhosale, *et al.*, 2018) in a similar
200 manner to low temperatures. Thus, *APOLO*-WRKY42 interaction was validated by RNA immuno-precipita-
201 tion (RIP-qPCR) in tobacco leaves and in *Arabidopsis* plants transitory or stably transformed with
202 35S:*WRKY42:GFP*, respectively (**Figure 3A**). Interestingly, according to the Arabidopsis eFP Browser

203 (Waese et al., 2017), *WRKY42* is induced in roots when seedlings are subjected to 4°C for 24h (**Figure 3B**).
204 At 10°C, we observed that *WRKY42* transcriptional accumulation augments significantly in roots (**Figure**
205 **3C**). Notably, 13 out of the 17 *APOLO* targets contained between 1 and 4 canonical WRKY TF binding sites
206 (W-box) in their promoters, including *RHD6* (**Supplementary Table 1**). By using a *35S:WRKY42:GFP* line,
207 we determined that WRKY42 can directly bind to the promoter region of *RHD6* (**Figure 3D**). Accordingly,
208 the over-expression of *WRKY42* (*35S:WRKY42:GFP* line) led to a basal increase of *RHD6* levels (**Figure 3E**)
209 and RH elongation (**Figure 3F**) at ambient temperature, mimicking the effect of cold. On the contrary, cold-
210 mediated induction of *RHD6* is abolished in the *wrky42* mutant ((Su et al., 2015); **Figure 3E**), which con-
211 sistently exhibits shorter RHs at 22°C and almost no RH elongation at low temperatures (**Figure 3F**). Taken
212 together, these results suggest that the *APOLO*-interacting TF WRKY42 is an important regulator of *RHD6*-
213 mediated RH growth in response to cold.

214 We thus wondered to what extent WRKY42 regulates the epigenetic landscape of the *RHD6* locus.
215 We first observed that H3K27me3 deposition over *RHD6* is significantly augmented in the *wrky42* mutant
216 background, in contrast to *AZG2*, an *APOLO* target non-related to WRKY42 (**Figure 4A**), consistent with
217 reduced *RHD6* basal levels reported in *wrky42* (**Figure 3E**). Therefore, we evaluated the mutual contribu-
218 tion of *APOLO* and WRKY42 to their respective recognition of the *RHD6* locus. *APOLO* ChIRP-qPCR in the
219 WT and *wrky42* mutant (**Figure 4B**) revealed similar binding to *RHD6*, indicating that WRKY42 does not
220 participates in *APOLO*-target recognition. Reciprocally, we assessed the control of *APOLO* over WRKY42
221 recognition of the *RHD6* locus. To this end, chromatin was extracted from *35S:WRKY42:GFP* seedlings and
222 increasing amounts of *in vitro* transcribed *APOLO* were added before cross-link and regular WRKY42 ChIP
223 over *RHD6*. Strikingly, increasing concentrations of *APOLO* gradually decoy WRKY42 away from the *RHD6*
224 locus (**Figure 4C**), hinting at a stoichiometric regulation of *APOLO* over the activity of its partner TF.

225 Collectively, our results indicate that the regulation of *RHD6* expression in response to cold
226 depends on Polycomb-dependent H3K27me3 dynamic deposition. The WRKY42-*APOLO* complex
227 modulates the epigenetic environment of *RHD6*, activating its transcription and promoting RH growth at
228 low temperatures. *RHD6* activation further triggers the expression of *RSL2* and *RSL4* that control the
229 transcriptional RH program inducing cell expansion in response to cold (**Figure 4D**).

230

231 **DISCUSSION**

232 Cell fate determination in the epidermis has been extensively studied (Ryu et al., 2005; Song et al.,
233 2011; Schiefelbein et al., 2014; Balcerowicz et al., 2015). Once trichoblast cells differentiate in the root

234 epidermis, RHs develop as fast polar growing protuberances in response to endogenous and environmen-
235 tal signals (Menand et al., 2007; Yi et al., 2010; Pires et al., 2013; Marzol et al., 2017) . RHs are one of the
236 main entry points in the roots for water-soluble macronutrients, such as Pi and nitrates. Pi is an essential
237 element for plant growth and development, and the availability of this macronutrient is a factor limiting
238 plant productivity. In Arabidopsis roots, low Pi in the soil triggers auxin synthesis and transport, enhancing
239 RH elongation to promote Pi uptake (Bhosale et al., 2018). Thus, auxin mediates low Pi-induced promotion
240 of RH cell expansion. Under low soil Pi, auxin synthesis is enhanced specifically in the root cap (Stepanova
241 et al., 2008) and transported (mostly by AUX1, PIN2, and PGP4) from the apex to the differentiation zone,
242 specifically leading to an increase of auxin levels in trichoblasts (Jones et al., 2009; Bhosale et al., 2018;
243 Wang et al., 2020) . In response to the high-auxin microenvironment, RHs protrude from the root epider-
244 mis controlled by RHD6 and RSL1(Menand et al., 2007; Pires et al., 2013) . High levels of auxin in tricho-
245 blasts trigger a signaling cascade mediated by TIR1-ARF19 (and possibly also ARF7) that directly induce the
246 expression of *RSL4* (and likely of *RSL2*) and promote RH elongation (Yi et al., 2010; Mangano et al., 2017;
247 Mangano et al., 2018b; Bhosale et al., 2018). ARF7 and ARF19 also activate other RH genes independently
248 of RSL4 (Schoenaers et al., 2018). Interestingly, our results indicate that the lncRNA *APOLO* participates in
249 the response to low temperatures. *APOLO* is directly activated by ARF7 and regulates the transcriptional
250 activity of its neighboring gene *PINOID* (*PID*) by shaping local 3D chromatin conformation (Ariel et al., 2014;
251 Ariel et al., 2020). *PID* encodes a kinase responsible for accurate auxin polar transport by localizing PIN2 in
252 the root cell membrane (Friml et al., 2004). More recently, it was shown that *APOLO* can recognize a subset
253 of distant genes across the *Arabidopsis* genome, most of them being related to auxin synthesis and signal-
254 ling (Ariel et al., 2020). In this work, we demonstrate that a group of RH related genes are directly regulated
255 by *APOLO* in response to cold, including the RH master regulator *RHD6*. Collectively, our results uncover a
256 lncRNA-mediated epigenetic link between environmental signals and auxin homeostasis modulating RH
257 growth. Moreover, our observations suggest that low temperatures restrict nutrient mobility and availabil-
258 ity in the culture medium, leading to the promotion of polar RH growth. Further research will be needed
259 to determine what is the limiting nutrient mediating the effect of cold on RH growth.

260 Although substantial progress has been achieved in the identification of the molecular actors con-
261 trolling RH development, the impact of chromatin conformation in the transcriptional regulation of central
262 TFs remains poorly understood. In this study, we have revealed a new mechanism of gene regulation in
263 RHs by which the lncRNA *APOLO* integrates chromatin-associated ribonucleoprotein complexes together
264 with the TF WYRK42, participating in the transcriptional activation of *RHD6* and the downstream RH gene

265 network (**Figure 4D**). *APOLO* directly regulates the chromatin 3D conformation of the genomic region en-
266 compassing the *RHD6* locus and stoichiometrically recruits WYRK42, previously linked to Pi-starvation
267 (Chen et al., 2009; Su et al., 2015). Our results suggest that an *APOLO*-WRKY42 hub regulates RH cell elon-
268 gation through the master regulator RHD6, although the *APOLO*-WYRKY42 hub potentially targets several
269 additional cell wall related genes (**Supplementary Table 1**) at the end of the pathway controlled by RHD6
270 and the RHD6-downstream TFs RSL2/RSL4 (Mangano et al., 2017; Mangano et al., 2018a) .

271 Participation of epigenetic factors in root cell identity determination strongly suggests the default
272 pattern for epidermal cell fate that can be overridden by environmental stimuli (Guimil and Dunand, 2006).
273 Interestingly, it was reported that the expression of *GLABRA2* (*GL2*), a gene encoding a TF repressing *RHD6*
274 in atrichoblasts, is tightly regulated at the epigenetic level. By using 3D fluorescence *in situ* hybridization,
275 it was shown that alternative states of chromatin organization around the *GL2* locus are required to control
276 position-dependent cell-type specification in the root epidermis (Costa and Shaw, 2006) . Furthermore,
277 *GL2* epigenetic regulation was proposed to be responsive to salt stress (Beyrne et al., 2019). In addition, a
278 comprehensive characterization of alternative mutant lines uncovered the role of PRC2 in the regulation
279 of RH development (Ikeuchi et al., 2015). Loss-of-function mutants in different PRC2 subunits develop uni-
280 cellular RHs but fail to retain the differentiated state, generating a disorganized cell mass from each single
281 RH. It was shown that the resulting RHs are able to undergo a normal endoreduplication program, increas-
282 ing their nuclear ploidy, although they subsequently reinitiate mitotic division and successive DNA replica-
283 tion. It was proposed that aberrant RH development in PRC2 related mutants is due to the epigenetic
284 deregulation of key regulatory genes such as *WOUND INDUCED DEDIFFERENTIATION 3* (*WIND3*) and *LEAFY*
285 *COTYLEDON 2* (*LEC2*) (Ikeuchi et al., 2015). Here, we showed that the single mutants *clf* (PRC2) and *lhp1*
286 (PRC1) are affected in RH growth. Moreover, we showed that in the *clf* background H3K27me3 deposition
287 throughout the *RHD6* locus is partially impaired, and that *clf* mutant is affected in RH elongation promoted
288 by cold. Altogether, our results suggest that Polycomb proteins participate in the control of RH-related
289 genes transcriptional reprogramming at low temperatures.

290 Notably, CLF and LHP1 were shown to interact with a subset of lncRNAs in *Arabidopsis*, modulating
291 the activity of PRC target genes (Lucero et al., 2020). Interestingly, several lncRNAs have been linked to
292 the control of transcription in response to cold. *FLOWERING LOCUS C* is regulated by at least three lncRNAs.
293 First, the alternative splicing of a set of antisense transcripts, collectively named as *COOLAIR*, depends on
294 the prolonged exposure to cold, epigenetically repressing *FLC* (Marquardt et al., 2014). The use of the
295 *COOLAIR* proximal poly(A) site results in down-regulation of *FLC* expression in a process involving FLOW-
296 ERING LOCUS D (FLD), an H3K4me2 demethylase (Marquardt et al., 2014). A second lncRNA called *COLD*

297 *ASSISTED INTRONIC NONCODING RNA* (*COLDAIR*) is fully encoded in the sense strand of the first intron of
298 *FLC.* Similar to *COOLAIR*, its accumulation oscillates in response to low temperatures. It was proposed that
299 *COLDAIR* recruits the PRC2 component CLF to target *FLC* for H3K27me3 deposition (Heo and Sung, 2011).
300 More recently, a third lncRNA modulating *FLC* transcription was identified (Kim and Sung, 2017). The cold-
301 responsive lncRNA *COLDWRAP* is derived from the *FLC* proximal promoter and it also interacts with PRC2.
302 It was suggested that *COLDWRAP* functions in cooperation with the lncRNA *COLDAIR* to retain Polycomb
303 at the *FLC* promoter through the formation of a repressive intragenic chromatin loop (Kim and Sung, 2017).
304 Another lncRNA named *SVALKA* was shown to mediate the response to low temperatures (Kindgren et al.,
305 2018). Interestingly, the activation of *SVALKA* by cold triggers the transcription of a cryptic downstream
306 lncRNA, which overlaps the antisense locus of the *C-repeat/dehydration-responsive element Binding Fac-*
307 *tor 1* (*CBF1*), involved in the early response to cold in Arabidopsis. Antisense transcription causes Pol II
308 head-to-head collision modulating transcriptional termination of *CBF1* (Kindgren et al., 2018). Here, we
309 show that the auxin-responsive lncRNA *APOLO* is also transcriptionally modulated by cold. The differential
310 accumulation of 24nt siRNAs across the *APOLO* locus at low temperatures indicates that this activation is
311 related to a decrease in RdDM. Moreover, we showed here that the intergenic region between *PID* and
312 *APOLO* acting as a divergent promoter is also activated at low temperatures in RHs, as revealed by the
313 reporter gene *GFP*. Thus, the lncRNA *APOLO* integrates external signals into auxin-dependent develop-
314 mental outputs in Arabidopsis.

315 In the last decade, lncRNAs have emerged as regulators of gene expression at different levels,
316 ranging from epigenetics to protein modifications and stability (Ariel et al., 2015). Notably, it has been
317 shown in animals that noncoding transcripts can be recognized by TFs. In humans, it was proposed that
318 the interaction with the lncRNA *SMALL NUCLEOLAR RNA HOST GENE 15* (*SNHG15*) stabilizes the TF Slug in
319 colon cancer cells. It was shown that *SNHG15* is recognized by the zinc finger domain of Slug preventing
320 its ubiquitination and degradation in living cells (Jiang et al., 2018). Also, the transcriptional activity of the
321 human gene *DIHYDROFOLATE REDUCTASE* (*DHFR*) is regulated by a lncRNA encoded in its proximal pro-
322 moter. It was proposed that the nascent noncoding transcript forms a hybrid with its parent DNA and
323 decoys the regulatory TF IIB away from the *DHFR* promoter, dissociating the transcriptional pre-initiation
324 complex in quiescent cells (Martianov et al., 2007). The lncRNA *P21 ASSOCIATED ncRNA DNA DAMAGE*
325 *ACTIVATED* (*PANDA*) was identified in human cancer and it was activated in response to DNA damage
326 (Hung et al., 2011). *PANDA* is transcribed from the promoter region of the *CDKN1A* gene and interacts with
327 the TF NF-YA to limit the expression of pro-apoptotic genes. The activity of *PANDA* has been linked to the
328 progression of different tumors (Kotake et al., 2016; Shi et al., 2019). Interestingly, it was shown that in

329 addition to NF-YA, *PANDA* interacts with the scaffold-attachment-factor A (SAFA) as well as PRC1 and PRC2
330 to modulate cell senescence. In proliferating cells, SAFA and *PANDA* recruit Polycomb components to re-
331 press the transcription of senescence-promoting genes. Conversely, the loss of SAFA–PANDA–PRC inter-
332 actions allows expression of the senescence program (Puvvula et al., 2014). In this work, we showed that
333 the PRC1-interacting lncRNA *APOLO* can also be recognized by the TF WRKY42, hinting at general lncRNA-
334 mediated mechanisms linking Polycomb complexes with the transcriptional machinery across kingdoms.
335 Furthermore, our observations indicate that the deregulation of *WRKY42* affects the epigenetic environ-
336 ment of *RHD6*. It was previously shown that the addition of *in vitro* transcribed *APOLO* to RNAi-*APOLO*
337 chromatin extracts was able to partially restore R-loop formation over *APOLO* target genes, and that high
338 levels of *APOLO* may titer LHP1 away from chromatin (Ariel et al., 2020). Here we show that the relative
339 accumulation of the lncRNA *APOLO* can modulate the binding activity of its partner TF to common target
340 genes. Collectively, our results strongly support that environmentally controlled cell fate in *Arabidopsis*
341 relies on a transcriptional reprogramming governed by a network of epigenetic regulatory complexes,
342 lncRNAs, TFs and effector proteins.
343
344 **MATERIALS AND METHODS**
345
346 **Plant Material and Growth Conditions.** All the *Arabidopsis thaliana* lines used were in the Columbia-0
347 (Col-0) background. *WRKY42* over expression transgenic plants were generated through *Agrobacterium*
348 *tumefaciens* (strain EHA105)-mediated transformation (Clough and Bent, 1998). *35S:WRKY42:GFP* trans-
349 formant lines were selected on MS/2 medium supplemented with kanamycin (40µg/mL) and *WRKY42* ex-
350 pression levels were measured by RT-qPCR (primers used are listed in **Supplementary Table 3**). The *wrky42*
351 mutant line belongs to the SALK collection (SALK_121674C), as the one previously characterized (Su et al.,
352 2015).The *rhd6-3/rsl1-1/rsl4-1*; *rsl2*; *rsl4*; *rsl2rsl4*, *35S:RSL4 and EXP7p:RSL4* transgenic lines were previ-
353 ously described and characterized (Yi et al., 2010; Hwang et al., 2017) Homozygous plants were obtained
354 in our laboratory and genotyped using the oligonucleotides indicated in **Supplementary Table 3**. Seeds
355 were surface sterilized and stratified at 4°C for 2d before being grown under long day conditions (16h light,
356 140µE.m^{-2}.sec^{-1}/8h dark), on ½-strength Murashige and Skoog media (1/2 MS) (Duchefa, Netherlands) with
357 0.8% plant agar (Duchefa, Netherlands).
358
359 **Cloning procedure.** The coding region of *WRKY42* (AT4G04450) excluding the STOP codon was amplified
360 by PCR, cloned into the Gateway entry vector pENTR/D-TOPO (Invitrogen) and recombined by Gateway

361 technology (LR reaction) into the pK7FWG2,0 vector containing a *p35S-GFP* cassette
362 (http://www.psb.ugent.be/gateway/index.php).
363
364 **Root hair phenotype characterization.** For quantitative analyses of RH phenotypes, 10 fully elongated RH
365 from the root elongation zone of 15-20 roots, were measured on the same conditions for each particular
366 case and grown on vertical plates with ½-strength Murashige and Skoog media (1/2 MS) (Duchefa, Neth-
367 erlands) and 0.8% plant agar (Duchefa, Netherlands) for 5 days at 22° and 3 days at 10°C. Measurements
368 were made after 8 days. Images were captured with an Olympus SZX7 Zoom Stereo Microscope (Olympus,
369 Japan) equipped with a Q-Colors digital camera and software Q Capture Pro 7(Olympus, Japan).
370
371 **Confocal microscopy analysis of root hairs.** Confocal laser scanning microscopy was performed using Zeiss
372 LSM5 Pascal (Zeiss, Germany) and a 40x water-immersion objective, N/A=1.2. Fluorescence was analyzed
373 by using 488 nm laser for GFP excitation (Laser Intensity: 70%, Detector Gain:550, Amplifier Offset:0.1,
374 Amplifier Gain:1), and emitted fluorescence was recorded between 490 and 525nm for GFP tag. Z stacks
375 were done with an optical slice of 1µm, and fluorescence intensity was measured in 15µm ROI (Region Of
376 Interest) at the RH tip and summed for quantification of fluorescence using ImageJ. Five replicates for each
377 of ten roots and 15 hairs per root were observed. Col-0 wild type root hairs were used as a negative con-
378 trol, to check autofluorescence signal occurrence and no signal were detected in the wavelengths range
379 stated above.
380
381 **RNA extraction and RT-qPCR.** Total RNA was extracted using TRIZol (Invitrogen) and 2 µg were subjected
382 to DNase treatment according to the manufacturer's protocol (Thermo Scientific). One µg of DNase-free
383 RNA was reverse transcribed using Maxima H Minus Reverse Transcriptase (Thermo Scientific). RT-qPCR
384 were performed using the LightCycler 480 SYBR Green I Master Kit on a LightCycler480 apparatus (Roche)
385 using standard protocols (40 cycles, 60°C annealing). *PP2A* (AT1G13320; primers are listed in **Supplemen-**
386 **tary Table 3**) was used as reference.
387
388 **RNA Immunoprecipitation.** RNA immunoprecipitation (RIP) assays were performed on transiently trans-
389 formed *N. benthamiana* leaves as described in (Sorenson and Bailey-Serres, 2015), or in 10-day-old *A. tha-*
390 *liana 35S:WRKY42:GFP* seedlings as described in (Bardou et al., 2014), using anti GFP (Abcam ab290) and
391 anti-IgG (Abcam ab6702). RIP was performed using Invitrogen Protein A Dynabeads. Precipitated RNAs
392 were prepared using TRI Reagent (Sigma-Aldrich), treated with DNase (Fermentas) and subjected to RT-

393 qPCR (High Capacity cDNA Reverse Transcription Kit (Thermo); primers used are listed in **Supplementary**
394 **Table 3**). Total RNAs were processed in parallel and considered the input sample.
395
396 **Chromatin Immunoprecipitation.** Chromatin immunoprecipitation (ChIP) assays were performed on 10-
397 day-old WT seedlings treated or not during 24h at 10 °C, using anti H3K27me3 (Diagenode pAb-195-050),
398 anti LHP1 (Covalab pab0923-P) and anti-IgG (Abcam ab6702), as described in (Ariel et al., 2020). Cross-
399 linked chromatin was sonicated using a water bath Bioruptor Pico (Diagenode; 30sec ON/30sec OFF pulses;
400 10 cycles; high intensity). ChIP was performed using Invitrogen Protein A Dynabeads. Precipitated DNA
401 was recovered using Phenol:Chloroform:Isoamilic Acid (25:24:1; Sigma) and subjected to RT-qPCR (primers
402 used are listed in **Supplementary Table 3**). Untreated sonicated chromatin was processed in parallel and
403 considered the input sample. For *in vitro* competition assays, *APOLO* was transcribed using the T7 tran-
404 scription kit (Promega; (Ariel et al., 2020)). After regular chromatin isolation from 10-day-old
405 *35S:WRKY42:GFP* seedlings, the sample was split in 4 independent tubes and diluted to 1ml in Nuclei Lysis
406 Buffer without SDS. 0 µg, 0.1 µg, 1 µg and 10 µg of *APOLO* were added to each sample respectively, and
407 incubated in rotation at 4 °C for 3h. Then, cross-linking was performed with 1% formaldehyde for 5 min at
408 4 °C, followed by 5 min with a final concentration of 50 mM glycine. SDS was added to a final concentration
409 of 0.1% prior to sonication and the subsequent steps of a regular ChIP protocol.
410
411 **Chromatin Isolation by RNA Purification followed by qPCR or mass spectrometry.** A method adapted
412 from the ChIRP protocol (Chu et al., 2012) was developed to allow the identification of plant DNA associ-
413 ated to specific lncRNAs, as described in (Ariel et al., 2014; Ariel et al., 2020). Briefly, plants were *in vivo*
414 crosslinked and cell nuclei were purified and extracted through sonication. The resulting supernatant was
415 hybridized against biotinylated complementary oligonucleotides that tile the lncRNA of interest and
416 lncRNA-associated chromatin was isolated using magnetic streptavidin beads. One hundred pmol of
417 probes against *APOLO* (ODD and EVEN set of probes (Ariel et al., 2014; Ariel et al., 2020)) and the corre-
418 sponding negative set against LacZ were used for independent purification. Co-purified ribonucleoprotein
419 complexes were eluted and used to purify RNA or DNA, which were later subjected to downstream assays
420 for quantification as previously described (Ariel et al., 2020).
421 The exploratory identification of plant nuclear proteins bound to *APOLO* was performed as described in
422 (Rigo et al., 2020). Plant samples were prepared as for ChIRP-qPCR. For protein extraction, approximately
423 250 g of 7-day-old Col-0 plants grown on solid half-strength MS medium was irradiated three times with
424 UV using a CROSSLINKERCL-508 (Uvitec) at 0.400 J/ cm^2. Protein purification samples for protein extraction

425 were DNase-treated according to the manufacturer (Thermo Scientific). After addition of 1.8ml of TCA-
426 acetone (5ml 6.1N TCA + 45ml acetone + 35µl β-mercaptoethanol), samples were incubated overnight at
427 -80°C. After centrifugation at 20000rpm for 20min at 4°C, the supernatant was discarded and 1.8ml of
428 acetone wash buffer (120ml acetone, 84µl β-mercaptoethanol) was added to the samples. Then, samples
429 were incubated 1h at -20°C and centrifuged again at 20000 rpm for 20min at 4°C. The supernatant was
430 discarded, and the dry pellet was used for mass spectrometry analyses.
431
432 **Chromatin Conformation Capture.** Chromosome conformation capture (3C) was performed basically as
433 previously described in (Ariel et al., 2020) starting with 2g of seedlings. Digestions were performed over-
434 night at 37°C with 400U *Dpn*II (NEB). DNA was ligated by incubation at 16°C for 5h in 4 ml volume using
435 100U of T4 DNA ligase (NEB). After reverse crosslinking and Proteinase K treatment (Invitrogen), DNA was
436 recovered by Phenol:Chloroform:Isoamilic Acid (25:24:1; Sigma) extraction and ethanol precipitation. Rel-
437 ative interaction frequency was calculated by qPCR (primers used are listed in **Supplementary Table 3**). A
438 region free of *Dpn*II was used to normalize the amount of DNA.
439
440 **Acknowledgments**
441 We thank Chang Liu for providing the Hi-C plot of Figure 2B. This work was supported by grants from
442 ANPCyT (PICT2016-0132 and PICT2017-0066) and Instituto Milenio iBio – Iniciativa Científica Milenio,
443 MINECON to JME; ANPCyT (PICT2016-0007 and PICT2016-0289) to FA; UNL (CAI+D 2016) to LL; Laboratoire
444 d'Excellence (LABEX) Saclay Plant Sciences (SPS; ANR-10-LABX-40) to MC; and CNRS (Laboratoire Interna-
445 tional Associé NOCOSYM) to MC and FA. LL, FI, JME and FA are researchers of CONICET; MM, JMP, CFF and
446 JRM are fellows of the same institution.
447
448 **Author contributions**
449 MM, JMP, LL, CFF, JRM, AC, MB and FA performed the experiments. JB, MB, FI, MC, JE and FA analyzed the
450 data. JE and FA conceived the project. FA, JE and CFF wrote the manuscript with the contribution of all
451 authors.
452
453 **References**
454 **Ariel, F., Jegu, T., Latrasse, D., Romero-Barrios, N., Christ, A., Benhamed, M., and Crespi, M.** (2014).
455 Noncoding transcription by alternative rna polymerases dynamically regulates an auxin-driven
456 chromatin loop. *Mol. Cell* **55**:383–396.

457 **Ariel, F., Romero-Barrios, N., Jégu, T., Benhamed, M., and Crespi, M.** (2015). Battles and hijacks:
458 Noncoding transcription in plants. *Trends Plant Sci.* **20**:362–371.
459 **Ariel, F., Lucero, L., Christ, A., Mammarella, M. F., Jegu, T., Veluchamy, A., Mariappan, K., Latrasse, D.,**
460 **Blein, T., Liu, C., et al.** (2020). R-Loop Mediated trans Action of the APOLO Long Noncoding RNA.
461 *Mol. Cell* **77**:1055-1065.e4.
462 **Balcerowicz, D., Schoenaers, S., and Vissenberg, K.** (2015). Cell Fate Determination and the Switch from
463 Diffuse Growth to Planar Polarity in Arabidopsis Root Epidermal Cells. *Front. Plant Sci.* **6**:1–13.
464 **Bardou, F., Ariel, F., Simpson, C. G., Romero-Barrios, N., Laporte, P., Balzergue, S., Brown, J. W. S., and**
465 **Crespi, M.** (2014). Long Noncoding RNA Modulates Alternative Splicing Regulators in Arabidopsis.
466 *Dev. Cell* **30**:166–176.
467 **Beyrne, C. C., Iusem, N. D., and González, R. M.** (2019). Effect of salt stress on cytosine methylation
468 within GL2, an Arabidopsis thaliana gene involved in root epidermal cell differentiation. Absence of
469 inheritance in the unstressed progeny. *Int. J. Mol. Sci.* **20**:1–13.
470 **Bhosale, R., Giri, J., Pandey, B. K., Giehl, R. F. H., Hartmann, A., Traini, R., Truskina, J., Leftley, N.,**
471 **Hanlon, M., Swarup, K., et al.** (2018). A mechanistic framework for auxin dependent Arabidopsis
472 root hair elongation to low external phosphate. *Nat. Commun.* **9**:1–9.
473 **Bruex, A., Kainkaryam, R. M., Wieckowski, Y., Kang, Y. H., Bernhardt, C., Xia, Y., Zheng, X., Wang, J. Y.,**
474 **Lee, M. M., Benfey, P., et al.** (2012). A Gene Regulatory Network for Root Epidermis Cell
475 Differentiation in Arabidopsis. *PLoS Genet.* **8**:1–20.
476 **Chen, Y. F., Li, L. Q., Xu, Q., Kong, Y. H., Wang, H., and Wu, W. H.** (2009). The WRKY6 transcription factor
477 modulates PHOSPHATE1 expression in response to low pi stress in arabidopsis. *Plant Cell* **21**:3554–
478 3566.
479 **Chu, C., Quinn, J., and Chang, H. Y.** (2012). Chromatin isolation by RNA purification (ChIRP). *J. Vis. Exp.*
480 Advance Access published March 25, 2012, doi:10.3791/3912.
481 **Clough, S. J., and Bent, A. F.** (1998). Floral dip: a simplified method for Agrobacterium-mediated
482 transformation of Arabidopsis thaliana. *Plant J.* **16**:735–43.
483 **Costa, S., and Shaw, P.** (2006). Chromatin organization and cell fate switch respond to positional
484 information in Arabidopsis. *Nature* **439**:493–496.
485 **Datta, S., Prescott, H., and Dolan, L.** (2015). Intensity of a pulse of RSL4 transcription factor synthesis
486 determines Arabidopsis root hair cell size. *Nat. Plants* **1**:1–6.
487 **Devaiah, B. N., Karthikeyan, A. S., and Raghothama, K. G.** (2007). WRKY75 transcription factor is a
488 modulator of phosphate acquisition and root development in Arabidopsis. *Plant Physiol.* **143**:1789–

489 1801.
490 **Dong, J., Chen, C., and Chen, Z.** (2003). Expression profiles of the Arabidopsis WRKY gene superfamily
491 during plant defense response. *Plant Mol. Biol.* **51**:21–37.
492 **Franco-Zorrilla, J. M., Valli, A., Todesco, M., Mateos, I., Puga, M. I., Rubio-Somoza, I., Leyva, A., Weigel,**
493 **D., García, J. A., and Paz-Ares, J.** (2007). Target mimicry provides a new mechanism for regulation
494 of microRNA activity. *Nat. Genet.* **39**:1033–1037.
495 **Friml, J., Yang, X., Michniewicz, M., Weijers, D., Quint, A., Tietz, O., Benjamins, R., Ouwerkerk, P. B. F.,**
496 **Ljung, K., Sandberg, G., et al.** (2004). A PINOID-dependent binary switch in apical-basal PIN polar
497 targeting directs auxin efflux. *Science* **306**:862–5.
498 **Guimil, S., and Dunand, C.** (2006). Patterning of Arabidopsis epidermal cells: epigenetic factors regulate
499 the complex epidermal cell fate pathway. *Trends Plant Sci.* **11**:601–609.
500 **Gyula, P., Baksa, I., Tóth, T., Mohorianu, I., Dalmay, T., and Szittya, G.** (2018). Ambient temperature
501 regulates the expression of a small set of sRNAs influencing plant development through NF-YA2 and
502 YUC2. *Plant Cell Environ.* **41**:2404–2417.
503 **Heo, J. B., and Sung, S.** (2011). Vernalization-mediated epigenetic silencing by a long intronic noncoding
504 RNA. *Science (80-.).* **331**:76–9.
505 **Hung, T., Wang, Y., Lin, M. F., Koegel, A. K., Kotake, Y., Grant, G. D., Horlings, H. M., Shah, N.,**
506 **Umbricht, C., Wang, P., et al.** (2011). Extensive and coordinated transcription of noncoding RNAs
507 within cell-cycle promoters. In *Nature Genetics*, pp. 621–629. NIH Public Access.
508 **Hwang, Y., Choi, H. S., Cho, H. M., and Cho, H. T.** (2017). Tracheophytes contain conserved orthologs of
509 a basic helix-loop-helix transcription factor that modulate ROOT HAIR SPECIFIC genes. *Plant Cell*
510 **29**:39–53.
511 **Ikeuchi, M., Iwase, A., Rymen, B., Harashima, H., Shibata, M., Ohnuma, M., Breuer, C., Morao, A. K., De**
512 **Lucas, M., De Veylder, L., et al.** (2015). PRC2 represses dedifferentiation of mature somatic cells in
513 Arabidopsis. *Nat. Plants* **1**:1–7.
514 **Jabnoune, M., Secco, D., Lecampion, C., Robaglia, C., Shu, Q., and Poirier, Y.** (2013). A Rice cis-Natural
515 antisense RNA acts as a translational enhancer for its cognate mRNA and contributes to phosphate
516 homeostasis and plant fitness. *Plant Cell* **25**:4166–4182.
517 **Jiang, H., Li, T., Qu, Y., Wang, X., Li, B., Song, J., Sun, X., Tang, Y., Wan, J., Yu, Y., et al.** (2018). Long non-
518 coding RNA SNHG15 interacts with and stabilizes transcription factor Slug and promotes colon
519 cancer progression. *Cancer Lett.* **425**:78–87.
520 **Jones, A. R., Kramer, E. M., Knox, K., Swarup, R., Bennett, M. J., Lazarus, C. M., Leyser, H. M. O., and**

521 **Grierson, C. S.** (2009). Auxin transport through non-hair cells sustains root-hair development. *Nat.*
522 *Cell Biol.* **11**:78–84.
523 **Karas, B., Amyot, L., Johansen, C., Sato, S., Tabata, S., Kawaguchi, M., and Szczyglowski, K.** (2009).
524 Conservation of Lotus and Arabidopsis basic helix-loop-helix proteins reveals new players in root
525 hair development. *Plant Physiol.* **151**:1175–1185.
526 **Kim, D. H., and Sung, S.** (2017). Vernalization-Triggered Intragenic Chromatin Loop Formation by Long
527 Noncoding RNAs. *Dev. Cell* **40**:302-312.e4.
528 **Kindgren, P., Ard, R., Ivanov, M., and Marquardt, S.** (2018). Transcriptional read-through of the long
529 non-coding RNA SVALKA governs plant cold acclimation. *Nat. Commun.* **9**:1–11.
530 **Kotake, Y., Kitagawa, K., Ohhata, T., Sakai, S., Uchida, C., Niida, H., Naemura, M., and Kitagawa, M.**
531 (2016). Long Non-coding RNA, PANDA, Contributes to the Stabilization of p53 Tumor Suppressor
532 Protein. *Anticancer Res.* **36**:1605–11.
533 **Lamport, D. T. A., Kieliszewski, M. J., Chen, Y., and Cannon, M. C.** (2011). Role of the Extensin
534 Superfamily in Primary Cell Wall Architecture. *Plant Physiol.* **156**:11–19.
535 **Lin, Q., Ohashi, Y., Kato, M., Tsuge, T., Gu, H., Qu, L. J., and Aoyama, T.** (2015). GLABRA2 directly
536 suppresses basic helix-loop-helix transcription factor genes with diverse functions in root hair
537 development. *Plant Cell* **27**:2894–2906.
538 **Liu, C., Wang, C., Wang, G., Becker, C., Zaidem, M., and Weigel, D.** (2016). Genome-wide analysis of
539 chromatin packing in Arabidopsis thaliana at single-gene resolution. *Genome Res.* **26**:1057–1068.
540 **Lucero, L., Fonouni-Farde, C., Crespi, M., and Ariel, F.** (2020). Long noncoding RNAs shape transcription
541 in plants. *Transcription* Advance Access published May 14, 2020,
542 doi:10.1080/21541264.2020.1764312.
543 **Mangano, S., Denita-Juarez, S. P., Choi, H. S., Marzol, E., Hwang, Y., Ranocha, P., Velasquez, S. M.,**
544 **Borassi, C., Barberini, M. L., Aptekmann, A. A., et al.** (2017). Molecular link between auxin and
545 ROS-mediated polar growth. *Proc. Natl. Acad. Sci. U. S. A.* **114**:5289–5294.
546 **Mangano, S., Martínez Pacheco, J., Marino-Buslje, C., and Estevez, J. M.** (2018a). How Does pH Fit in
547 with Oscillating Polar Growth? *Trends Plant Sci.* **23**:479–489.
548 **Mangano, S., Denita-Juarez, S. P., Marzol, E., Borassi, C., and Estevez, J. M.** (2018b). High Auxin and
549 High Phosphate Impact on RSL2 Expression and ROS-Homeostasis Linked to Root Hair Growth in
550 Arabidopsis thaliana. *Front. Plant Sci.* **9**:1–8.
551 **Marquardt, S., Raitskin, O., Wu, Z., Liu, F., Sun, Q., and Dean, C.** (2014). Functional Consequences of
552 Splicing of the Antisense Transcript COOLAIR on FLC Transcription. *Mol. Cell* **54**:156–165.

553 **Martianov, I., Ramadass, A., Serra Barros, A., Chow, N., and Akoulitchev, A.** (2007). Repression of the
554 human dihydrofolate reductase gene by a non-coding interfering transcript. *Nature* **445**:666–670.
555 **Marzol, E., Borassi, C., Denita Juárez, S. P., Mangano, S., and Estevez, J. M.** (2017). RSL4 Takes Control:
556 Multiple Signals, One Transcription Factor. *Trends Plant Sci.* **22**:553–555.
557 **Marzol, E., Borassi, C., Bringas, M., Sede, A., Rodríguez Garcia, D. R., Capece, L., and Estevez, J. M.**
558 (2018). Filling the Gaps to Solve the Extensin Puzzle. *Mol. Plant* **11**:645–658.
559 **Menand, B., Yi, K., Jouannic, S., Hoffmann, L., Ryan, E., Linstead, P., Schaefer, D. G., and Dolan, L.**
560 (2007). An ancient mechanism controls the development of cells with a rooting function in land
561 plants. *Science (80-.).* **316**:1477–1480.
562 **Pires, N. D., Yi, K., Breuninger, H., Catarino, B., Menand, B., and Dolan, L.** (2013). Recruitment and
563 remodeling of an ancient gene regulatory network during land plant evolution. *Proc. Natl. Acad. Sci.*
564 *U. S. A.* **110**:9571–9576.
565 **Puvvula, P. K., Desetty, R. D., Pineau, P., Marchio, A., Moon, A., Dejean, A., and Bischof, O.** (2014). Long
566 noncoding RNA PANDA and scaffold-attachment-factor SAFA control senescence entry and exit.
567 *Nat. Commun.* **5**:1–16.
568 **Rigo, R., Bazin, J., Romero-Barrios, N., Moison, M., Lucero, L., Christ, A., Benhamed, M., Blein, T.,**
569 **Huguet, S., Charon, C., et al.** (2020). *An Arabidopsis long noncoding RNA modulates the*
570 *transcriptome through interactions with a network of splicing factors*. Cold Spring Harbor
571 Laboratory.
572 **Ringli, C.** (2010). The hydroxyproline-rich glycoprotein domain of the Arabidopsis LRX1 requires Tyr for
573 function but not for insolubilization in the cell wall. *Plant J.* **63**:662–669.
574 **Ryu, K. H., Kang, Y. H., Park, Y. H., Hwang, I., Schiefelbein, J., and Lee, M. M.** (2005). The WEREWOLF
575 MYB protein directly regulates CAPRICE transcription during cell fate specification in the
576 Arabidopsis root epidermis. *Development* **132**:4765–4775.
577 **Schiefelbein, J., Huang, L., and Zheng, X.** (2014). Regulation of epidermal cell fate in Arabidopsis roots:
578 the importance of multiple feedback loops. *Front. Plant Sci.* **5**:1–4.
579 **Schoenaers, S., Balcerowicz, D., Breen, G., Hill, K., Zdanio, M., Mouille, G., Holman, T. J., Oh, J., Wilson,**
580 **M. H., Nikonorova, N., et al.** (2018). The Auxin-Regulated CrRLK1L Kinase ERULUS Controls Cell
581 Wall Composition during Root Hair Tip Growth. *Curr. Biol.* **28**:722-732.e6.
582 **Shi, W., Wang, Q., Bian, Y., Fan, Y., Zhou, Y., Feng, T., Li, Z., and Cao, X.** (2019). Long noncoding RNA
583 PANDA promotes esophageal squamous carcinoma cell progress by dissociating from NF-YA but
584 interact with SAFA. *Pathol. Res. Pract.* **215**:1–11.

585 **Song, S. K., Ryu, K. H., Kang, Y. H., Song, J. H., Cho, Y. H., Yoo, S. D., Schiefelbein, J., and Lee, M. M.**
586 (2011). Cell fate in the Arabidopsis root epidermis is determined by competition between
587 WEREWOLF and CAPRICE. *Plant Physiol.* **157**:1196–1208.
588 **Sorenson, R., and Bailey-Serres, J.** (2015). Rapid immunopurification of ribonucleoprotein complexes of
589 plants. *Methods Mol. Biol.* **1284**:209–219.
590 **Stepanova, A. N., Robertson-Hoyt, J., Yun, J., Benavente, L. M., Xie, D. Y., Doležal, K., Schlereth, A.,**
591 **Jürgens, G., and Alonso, J. M.** (2008). TAA1-Mediated Auxin Biosynthesis Is Essential for Hormone
592 Crosstalk and Plant Development. *Cell* **133**:177–191.
593 **Su, T., Xu, Q., Zhang, F. C., Chen, Y., Li, L. Q., Wu, W. H., and Chen, Y. F.** (2015). WRKY42 Modulates
594 phosphate homeostasis through regulating phosphate translocation and acquisition in Arabidopsis.
595 *Plant Physiol.* **167**:1579–1591.
596 **Velasquez, S. M., Ricardi, M. M., Dorosz, J. G., Fernandez, P. V., Nadra, A. D., Pol-Fachin, L., Egelund, J.,**
597 **Gille, S., Harholt, J., Ciancia, M., et al.** (2011). O-glycosylated cell wall proteins are essential in root
598 hair growth. *Science (80-.).* **332**:1401–1403.
599 **Velasquez, S. M., Marzol, E., Borassi, C., Pol-Fachin, L., Ricardi, M. M., Mangano, S., Juarez, S. P. D.,**
600 **Salter, J. D. S., Dorosz, J. G., Marcus, S. E., et al.** (2015). Low Sugar Is Not Always Good: Impact of
601 Specific O -Glycan Defects on Tip Growth in Arabidopsis. *Plant Physiol.* **168**:808–813.
602 **Veluchamy, A., Jégu, T., Ariel, F., Latrasse, D., Mariappan, K. G., Kim, S.-K., Crespi, M., Hirt, H.,**
603 **Bergounioux, C., Raynaud, C., et al.** (2016). LHP1 Regulates H3K27me3 Spreading and Shapes the
604 Three-Dimensional Conformation of the Arabidopsis Genome. *PLoS One* **11**:1–25.
605 **Vijayakumar, P., Datta, S., and Dolan, L.** (2016). ROOT HAIR DEFECTIVE SIX-LIKE4 (RSL4) promotes root
606 hair elongation by transcriptionally regulating the expression of genes required for cell growth.
607 *New Phytol.* **212**:944–953.
608 **Waese, J., Fan, J., Pasha, A., Yu, H., Fucile, G., Shi, R., Cumming, M., Kelley, L. A., Sternberg, M. J.,**
609 **Krishnakumar, V., et al.** (2017). ePlant: Visualizing and exploring multiple levels of data for
610 hypothesis generation in plant biology. *Plant Cell* **29**:1806–1821.
611 **Wang, H., Xu, Q., Kong, Y. H., Chen, Y., Duan, J. Y., Wu, W. H., and Chen, Y. F.** (2014). Arabidopsis
612 WRKY45 transcription factor activates Phosphate transporter1;1 expression in response to
613 phosphate starvation. *Plant Physiol.* **164**:2020–2029.
614 **Wang, Q., Qin, G., Cao, M., Chen, R., He, Y., Yang, L., Zeng, Z., Yu, Y., Gu, Y., Xing, W., et al.** (2020). A
615 phosphorylation-based switch controls TAA1-mediated auxin biosynthesis in plants. *Nat. Commun.*
616 **11**:1–10.

617 **Won, S. K., Lee, Y. J., Lee, H. Y., Heo, Y. K., Cho, M., and Cho, H. T.** (2009). cis-element- and
618 transcriptome-based screening of root hair-specific genes and their functional characterization in
619 Arabidopsis. *Plant Physiol.* **150**:1459–1473.
620 **Xu, W., Li, K., Li, S., Hou, Q., Zhang, Y., Liu, K., and Sun, Q.** (2020). The R-Loop Atlas of Arabidopsis
621 Development and Responses to Environmental Stimuli. *Plant Cell* **32**:888–903.
622 **Yi, K., Menand, B., Bell, E., and Dolan, L.** (2010). A basic helix-loop-helix transcription factor controls cell
623 growth and size in root hairs. *Nat. Genet.* **42**:264–267.
624 **Zhang, T. Q., Xu, Z. G., Shang, G. D., and Wang, J. W.** (2019). A Single-Cell RNA Sequencing Profiles the
625 Developmental Landscape of Arabidopsis Root. *Mol. Plant* **12**:648–660.

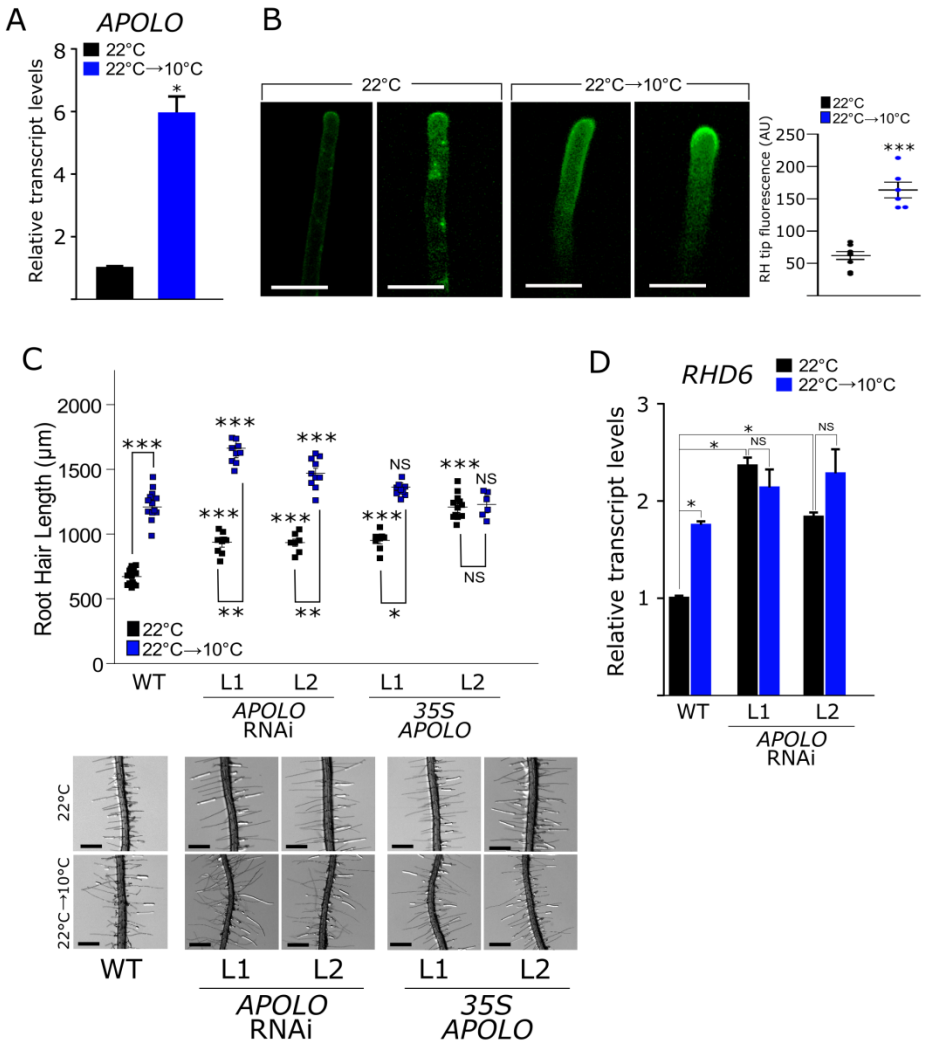

Figure 1. *APOLO* regulates root hair elongation in response to low temperatures

A. *APOLO* transcript levels measured by RT-qPCR in roots of 10-day-old plants grown at 22 °C treated or not for 24h at 10 °C.

B. The *APOLO* promoter region (full intergenic region between *PID* and *APOLO*) is active in root hairs at 22 °C and 10 °C, using the *GFP* reporter gene. Images are representative of the lowest and highest GFP signal detected in the observation of several roots. The quantification of the fluorescence is shown in the right panel.

C. Quantification of RH length of 8-day-old WT, RNAi-*APOLO* and *35S:APOLO* plants, respectively, at 22 °C and 10 °C. Each point is the mean ±error of the length of the 10 longest RHs identified in the root elongation zone in a single root. Representative images of each genotype are shown below the graph. Asterisks indicate significant differences between WT and the corresponding genotype at the same temperature or significant differences between temperature treatments on the same genotype at the same temperature (one way ANOVA followed by a Tukey-Kramer test; "*"<0.05, "**"<0.01, "***"<0.001). NS stands for no statistically significant difference.

D. *RHD6* transcript levels measured by RT-qPCR in roots of WT plants vs. two independent RNAi-*APOLO* lines grown at 22 °C treated or not for 24h at 10 °C.

643 In A and D, the error bar represents the SD of 3 biological replicates. The asterisk indicates that the differ-
644 ence is significant (t test $p<0.05$). Values are normalized using the constant housekeeping transcript *PP2A*.

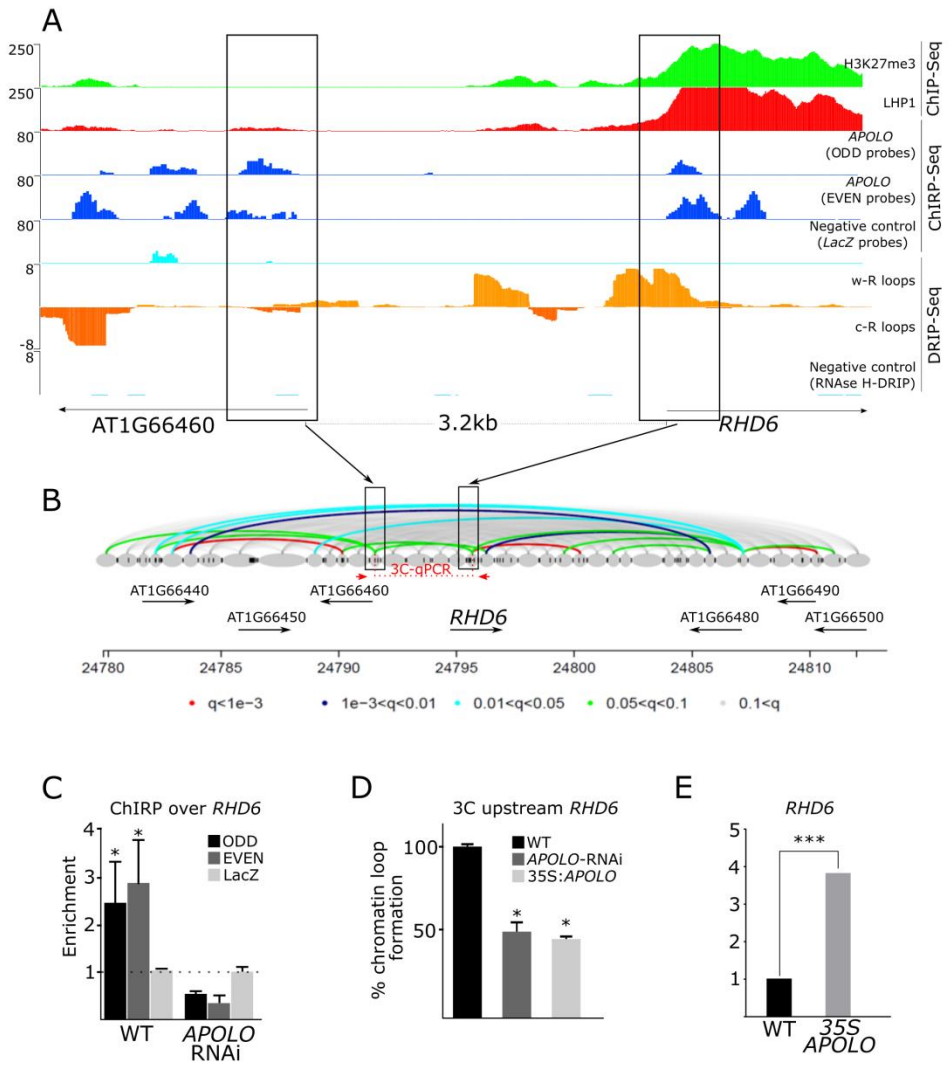

Figure 2. *APOLO* directly modulates chromatin three-dimensional conformation of the *RHD6* locus

A. Epigenomic landscape of the *RHD6* locus. Lane 1: H3K27me3 deposition by ChIP-Seq (Veluchamy et al., 2016). Lane 2: LHP1 deposition by ChIP-Seq (Veluchamy et al., 2016). Lane 3 to 5: *APOLO* recognition by ChIRP-Seq (Lane 3 and 4, using ODD and EVEN sets of probes against *APOLO*, respectively; Lane 5, negative control using LacZ probes)(Ariel et al., 2020). Lane 6 to 8: R-loop formation by DRIP-Seq (R-loop Atlas, root samples,(Xu et al., 2020), on Watson strand (Lane 6) and Crick strand (Lane 7). DRIP negative control after RNAseH treatment is shown in Lane 8. Gene annotation is shown at the bottom.

B. Chromatin loops identified in the *RHD6* region by *Dpn*II HiC (Liu et al., 2016). Colors of the loops are related to the corresponding q-values indicated below. Black boxes in A and B indicate the same genomic locations, where the bases of the chromatin loop correlate with R-loop formation and *APOLO* recognition (compared to gene annotations). In red the arrows indicate the position of the probes used for 3C-qPCR shown in **D**.

C. *APOLO* association to DNA of the *RHD6* locus by ChIRP-qPCR in WT and RNAi-*APOLO* plants. The background level was determined using a set of probes against LacZ RNA.

D. Relative chromatin loop formation by 3C-qPCR deduced from **B**, in WT plants vs. *35S:APOLO* and RNAi lines for the region upstream *RHD6*. The probes used for 3C-qPCR are indicated in red in panel **B**.

662 **E.** *RHD6* transcript levels revealed by RNA-Seq of WT vs. *35S:APOLO* plants(Ariel et al., 2020).
663 In C and D, the error bar represents the SD of 3 biological replicates. The asterisk indicates that the dif-
664 ference is significant (t test "*"<0.05, "***"<0.001).

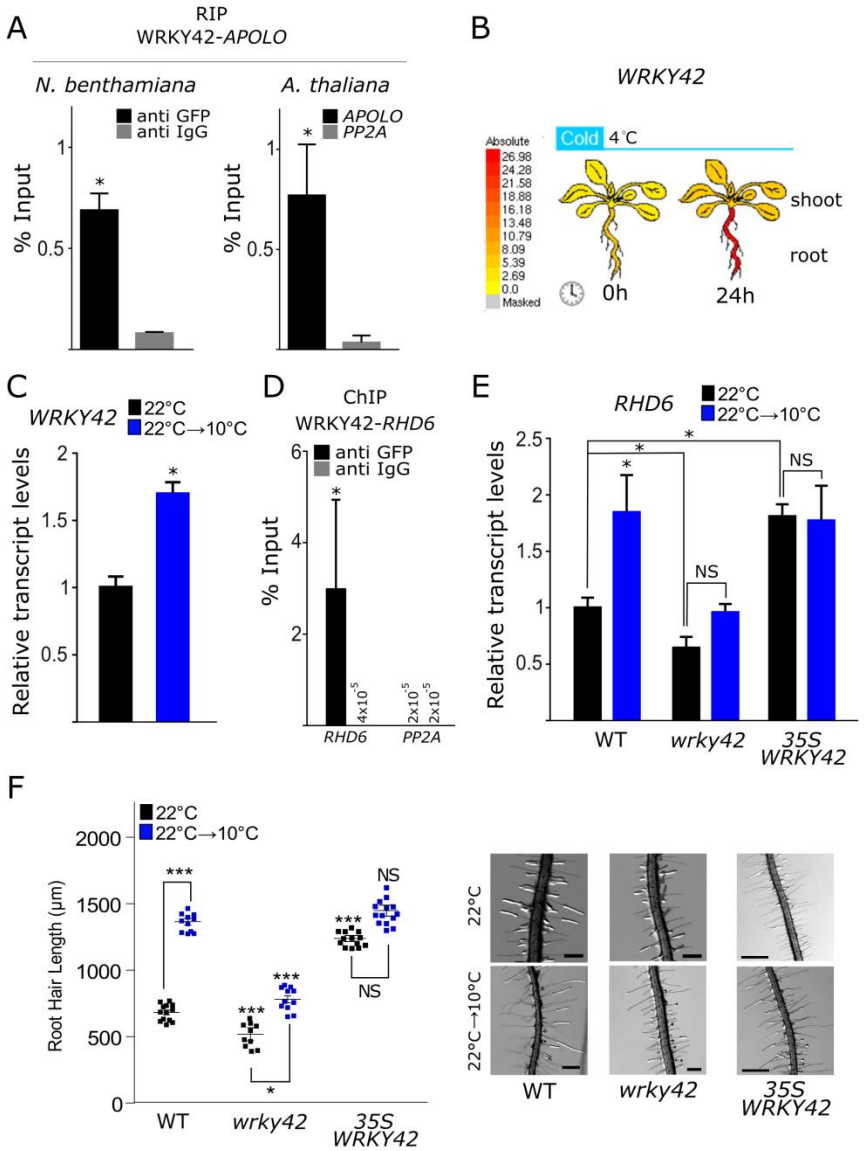

Figure 3. The transcription factor WRKY42 interacts with *APOLO* and directly regulates *RHD6* and participates in the response to cold

A. *APOLO*-WRKY42 interaction *in vivo* demonstrated by RNA Immunoprecipitation (RIP)-qPCR in transiently transformed tobacco leaves and stably transformed Arabidopsis plants. In tobacco, WRKY42:GFP and *APOLO* were co-transformed under the control of the 35S constitutive promoter. In Arabidopsis, *35S:WRKY42:GFP* transformed plants were used to detect the interaction with endogenous *APOLO*. Anti-IgG antibodies were used as a negative control. The RNA *PP2A* was considered as a RIP negative control in Arabidopsis plants.

B. Arabidopsis eFP Browser (Waese et al., 2017) plot representing the increase of *WRKY42* transcript levels in roots of seedlings treated for 24h at 4°C.

C. *WRKY42* transcript levels measured by RT-qPCR in roots of plants grown at 22°C treated or not for 24h at 10°C.

678 **D.** Chromatin Immunoprecipitation (ChIP)-qPCR assay revealing regulation by WRKY42 of *RHD6* by direct
679 recognition of its promoter region. Probes amplifying *PP2A* were used as a negative control of the experi-
680 ment. Anti-IgG antibodies were used as a negative control for each pair of probes.
681 **E.** *RHD6* transcript levels measured by RT-qPCR in roots of WT plants vs. *wrky42* mutants and
682 *35S:WRKY42:GFP* lines grown at 22°C treated or not for 24h at 10°C.
683 **F.** Quantification of RH length of plants WT, *wrky42* and *35S:WRKY42:GFP* at 22°C and 10°C. Each point is
684 the mean of the length of the 10 longest RHs identified in a single root. Representative images of each
685 genotype are shown on the right. Asterisks indicate significant differences between WT and the corre-
686 sponding genotype at the same temperature (one way ANOVA followed by a Tukey-Kramer test; "*"<0.05,
687 "***"<0.001).
688 In A, C, D and E, the error bar represents the SD of 3 biological replicates. The asterisk indicates that the
689 difference is significant (t test p<0.05). NS stands for no statistically significant difference. Values are nor-
690 malized using the constant housekeeping transcript *PP2A*.

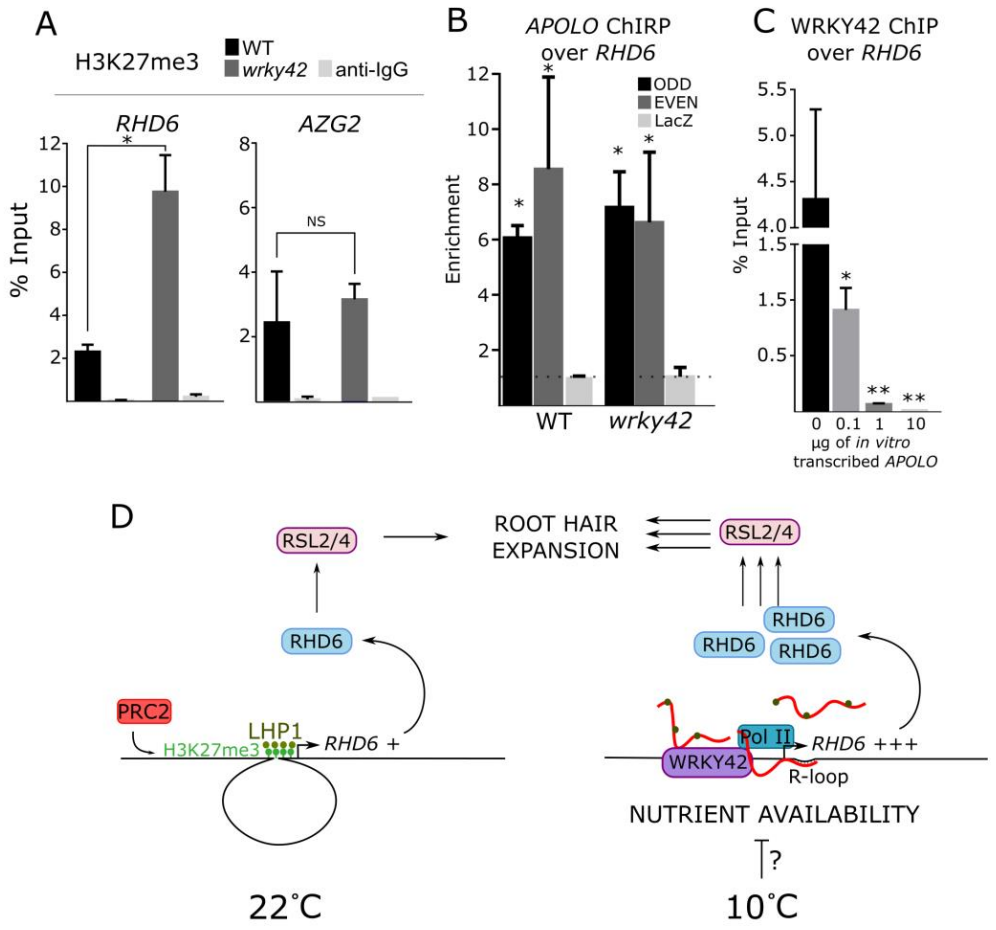

Figure 4. The WRKY42-*APOLO* hub activates *RHD6* transcription in response to low temperatures, promoting root hair expansion

A. H3K27me3 deposition in WT vs. *wrky42* mutant 10-day-old seedlings grown at 23°C over *RHD6* and a WRKY42-independent *APOLO* target (*AZG2*; (Ariel et al., 2020)). An immunoprecipitation (ChIP-qPCR) was performed using an anti-IgG antibody as a negative control.

B. *APOLO* association to DNA of the *RHD6* locus by ChIRP-qPCR in WT and *wrky42* mutant plants. The background level was determined using a set of probes against LacZ RNA.

C. WRKY42 immunoprecipitation over *RHD6* with the addition of increasing concentrations of *in vitro* transcribed *APOLO* prior to cross-linking.

D. Proposed model for the action of *APOLO* in RH growth under low temperatures. In response to cold, *APOLO* levels increase, recognizing the *RHD6* locus by sequence complementarity. Then, LHP1 is decoyed away from chromatin and H3K27me3 deposition decreases in a process involving WRKY42 and leading to the opening of the *RHD6* promoter region. Additionally, *APOLO* and WRKY42 jointly activate *RHD6* transcription. RHD6 activates the transcription of downstream TF genes *RSL2* and *4* promoting RH cell expansion.

In A, B and C the error bar represents the SD of 3 biological replicates. The asterisk indicates that the difference is significant (t test "*"<0.05, "**"<0.01).

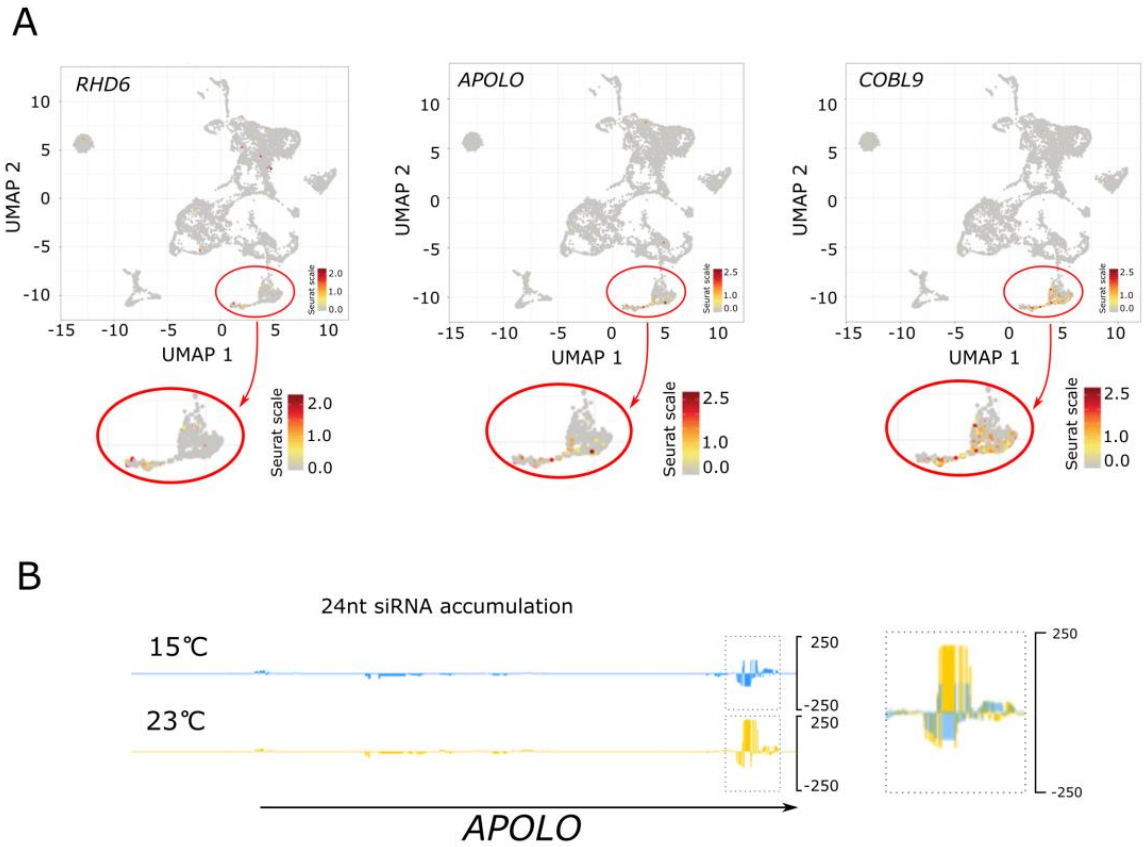

Supplementary Figure 1: *RHD6* and *APOLO* transcripts are enriched in root hair cells

A. Uniform Manifold Approximation and Projection (UMAP) clustering map of Arabidopsis root single cell RNA-seq ((Zhang et al., 2019); http://wanglab.sippe.ac.cn/rootatlas/) data. *RHD6*, *APOLO* and the trichoblast cell marker *COBL9* are respectively indicated in red in each plot.

B. 24nt siRNA accumulation over the *APOLO* locus revealed by small RNA-Seq of roots from WT seedlings grown at 15 °C or 23 °C (Gyula et al., 2018). On the right, a zoom of the 3' region is shown, with the overlapped signal at both temperatures.

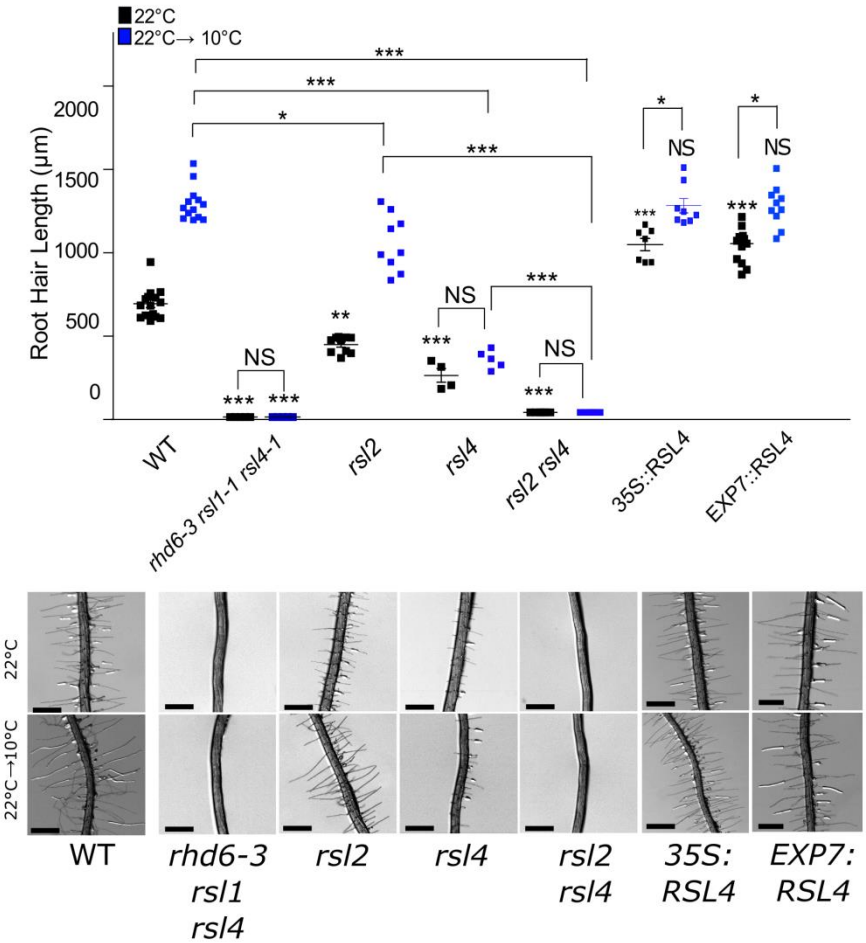

Supplementary Figure 2. Root hair expansion in response to cold is mediated by *RSL2* and *RSL4*
Quantification of RH length of plants WT, *rhd6-3, rsl1/4; rsl2; rsl4; rsl2/4*; *35S:RSL4* and *pEXP7:RSL4* at 22°C and 10°C. Each point is the mean ±error of the length of the 10 longest RHs identified in the root elongation zone in a single root. Representative images of each genotype are shown below the graph. Asterisks indicate significant differences between WT and the corresponding genotype at the same temperature or significant differences between temperature treatments on the same genotype at the same temperature (one way ANOVA followed by a Tukey-Kramer test; "*"<0.05, "**"<0.01, "***"<0.001), unless indicated differently. NS stands for no statistically significant difference.

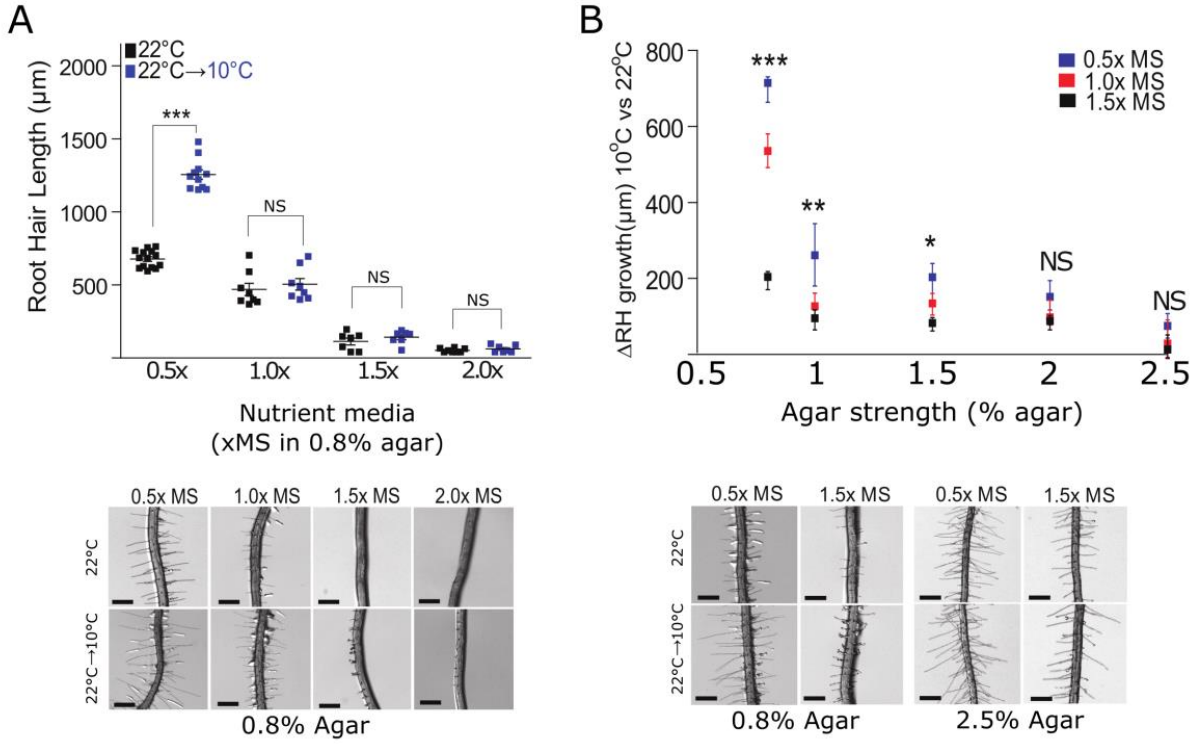

Supplementary Figure 3. Root hair expansion in response to cold seems to be related to nutrient availability

A. Quantification of RH length of WT plants at 22°C and 10°C at growing concentrations of Murashige and Skoog (MS) culture media. Each point is the mean ±error of the length of the 10 longest RHs identified in the root elongation zone in a single root. Representative images of each genotype are shown on the right. Asterisks indicate significant differences between temperature treatments on a specific nutrient media condition (one way ANOVA followed by a Tukey-Kramer test). NS stands for no statistically significant difference.

B. Quantification of RH length of WT plants expressed as the ratio between 10°C and 22°C at growing concentrations of MS culture media, for given concentrations of agar. Representative images of each genotype are shown below the graph. Each point is the mean ±error of the length of the 10 longest RHs identified in the root elongation zone in a single root. Asterisks indicate significant differences between agar percentage conditions (one way ANOVA followed by a Tukey-Kramer test; "*"<0.05, "**"<0.01, "***"<0.001). NS stands for no statistically significant difference.

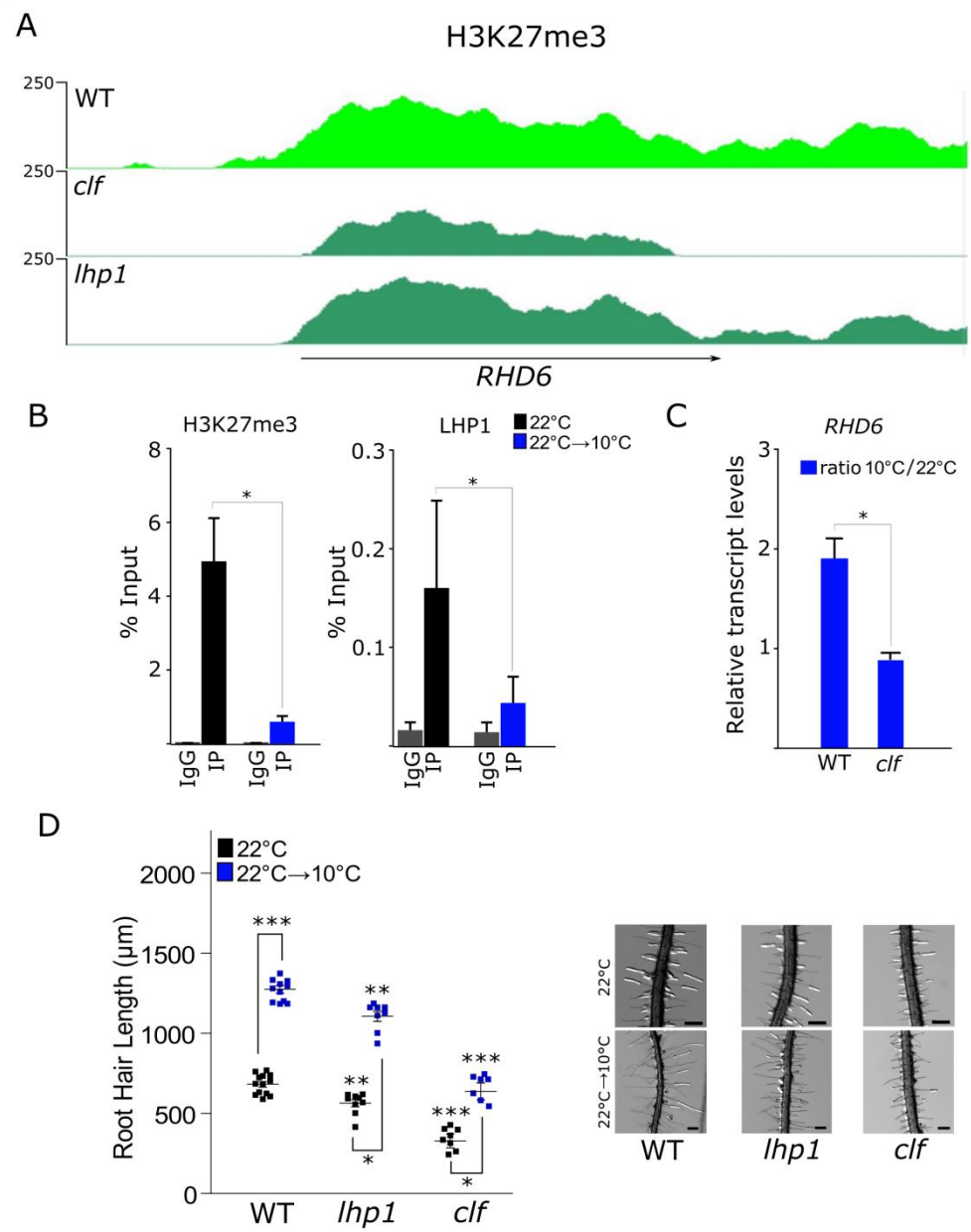

741
742
743 **Supplementary Figure 4: Induction of root hair elongation by low temperatures requires epigenetic Pol-**
744 **ycomb-mediated reprogramming**
745 **A.** H3K27me3 deposition across the *RHD6* locus in WT, *clf* and *lhp1* mutants, revealed by ChIP-seq from
746 seedlings grown at 23°C (Veluchamy et al., 2016).
747 **B.** H3K27me3 deposition measured by ChIP-qPCR over the *RHD6* locus in WT plants grown at 22°C treated
748 or not for 24h at 10°C. The negative control was performed using an anti-IgG antibody.
749 **C.** *RHD6* transcript levels measured by RT-qPCR in roots of WT plants vs. *clf* mutants, expressed as the ratio
750 between plants treated or not for 24h at 10°C over the mock plants grown at 22°C.
751 **D.** Quantification of RH length of plants WT, *lhp1* and *clf* at 22°C and 10°C. Each point is the mean ±error of
752 the length of the 10 longest RHs identified in the root elongation zone in a single root. Representative
753 images of each genotype are shown on the right. Asterisks indicate significant differences between WT and
754 the corresponding genotype at the same temperature or significant differences between temperature

755 treatments on the same genotype at the same temperature (one way ANOVA followed by a Tukey-Kramer
756 test; “**”<0.01, “***”<0.001).
757 In B and C, the error bar represents the SD of 3 biological replicates. The asterisk indicates that the differ-
758 ence is significant (t test p<0.05).

759 **LEGENDS TO SUPPLEMENTARY TABLES**
760
761 **Supplementary Table 1: *APOLO* targets related to root hair growth.**
762 The list of *APOLO bona fide* targets was determined in (Ariel et al., 2020). The search for root hairs-related
763 genes was performed based on (Won et al., 2009; Yi et al., 2010; Vijayakumar et al., 2016; Hwang et al.,
764 2017). LHP1 binding and H3K27me3 deposition was investigated in previously published datasets
765 (Veluchamy et al., 2016). W-boxes (TTGACY;(Dong et al., 2003)) present in the first 2500 bp upstream the
766 ATG of each gene was searched manually. The position of box is given only for *RHD6*, directly recognized
767 by WRKY42 (**Figure 4B**).
768
769 **Supplementary Table 2: Root hair-related genes deregulated in *35S:APOLO* seedlings.**
770 The list of deregulated genes was determined by RNA-Seq (Ariel et al., 2020). The search for root hairs-
771 related genes was performed based on (Won et al., 2009; Yi et al., 2010; Vijayakumar et al., 2016; Hwang
772 et al., 2017). Genes are classified as directly (same as in **Supplementary Table 1**) or indirectly regulated by
773 *APOLO*. *RHD6*, *RSL2* and *RSL4* are highlighted in red.
774
775 **Supplementary Table 3: List of oligonucleotides used in this work.**